Dynamics of modulated beams in spectral domain

Yampolsky, Nikolai

To be published in: Nuclear Instruments and Methods in Physics Research Section A: Accelerators, Spectrometers, Detectors and Associated Equipment

DOI to publisher's version: 10.1016/j.nima.2017.07.008

Permalink to record: http://permalink.lanl.gov/object/view?what=info:lanl-repo/lareport/LA-UR-17-27022

ARTICLE IN PRESS

Nuclear Inst. and Methods in Physics Research, A ▮ (▮▮▮▮) ▮▮▮–▮▮▮

Contents lists available at ScienceDirect

Nuclear Inst. and Methods in Physics Research, A

journal homepage: www.elsevier.com/locate/nima

Dynamics of modulated beams in spectral domain

Nikolai A. Yampolsky

Los Alamos National Laboratory, Los Alamos, NM, 87545, USA

ARTICLE INFO

Keywords:
Beam dynamics
Seeding schemes

ABSTRACT

General formalism for describing dynamics of modulated beams along linear beamlines is developed. We describe modulated beams with spectral distribution function which represents Fourier transform of the conventional beam distribution function in the 6-dimensional phase space. The introduced spectral distribution function is localized in some region of the spectral domain for nearly monochromatic modulations. It can be characterized with a small number of typical parameters such as the lowest order moments of the spectral distribution. We study evolution of the modulated beams in linear beamlines and find that characteristic spectral parameters transform linearly. The developed approach significantly simplifies analysis of various schemes proposed for seeding X-ray free electron lasers. We use this approach to study several recently proposed schemes and find the bandwidth of the output bunching in each case.

Published by Elsevier B.V.

1. Introduction

Free electron lasers (FELs) are the only currently available sources capable of generating coherent X-ray radiation. Presently several hard X-ray FELs (XFELs) are operated or under construction [1–5]. These light sources are designed to work in the Self-Amplified Spontaneous Emission (SASE) regime [6] which amplifies the shot noise within the FEL bandwidth. As a result, the output X-ray pulses have limited longitudinal coherence which may be undesirable for some applications. The XFEL performance can be strongly improved if it is seeded with coherent signal. Seeded FELs generate more powerful radiation with smaller bandwidth. That allows to design cheaper light sources having significantly larger brightness.

Growing FEL mode couples radiation with electron motion. Therefore, FEL can be seeded either with a narrowband radiation [7,8] or with an electron beam modulated at the X-ray wavelength [9–11]. The second option looks attractive since electrons are charged particles and they interact with electromagnetic fields unlike radiation which only weakly interacts with materials at X-ray frequencies. A large variety of available beam optics elements introduces a lot of options for transforming the modulation and controlling parameters of the output beam. Different schemes for generating modulated beams were recently proposed [9–13] and some were verified experimentally [14–16]. All these schemes utilize the same principle: first the beam is modulated and then the beam modulation is transformed in the following beamline to produce bunched beam. Conventional analysis of each scheme relies on following the electron trajectory in the phase space. Such an analysis is somewhat complicated and does not provide intuitive understanding of the scheme performance when the beamline parameters are changed. Moreover, such an approach does not allow one predicting the bandwidth of the resulting bunching if the initial modulation is not perfectly coherent. As a result, it is not clear whether the proposed schemes are suitable for the FEL seeding. In this paper we address this drawback and develop general formalism quantifying modulation parameters and describing evolution of a bunched beam along an arbitrary linear beamline. This approach simplifies the analysis and serves as a powerful tool for designing FEL seeding schemes.

The modulated beam has fine scale features in the phase space distribution. Low order moments of the beam distribution such as rms beam sizes, rms energy spread, *etc*. cannot capture these small scale variations. As a result, one needs to introduce high order moments to characterize the distribution function. That significantly complicates the analysis since the number of parameters characterizing the phase space distribution increases dramatically. Alternatively, one can consider the 6-dimensional (6D) Fourier transform of the beam distribution function, which introduces the spectral distribution function. Such a spectral distribution is well localized in some region of the spectral domain and it can be characterized with a small number of parameters such as the wavevector of the modulation and its bandwidth. These parameters capture the main properties of the modulation similar to the rms beam quantities which characterize its envelope. This approach is very similar to description of laser pulses which are commonly characterized with the carrier frequency and bandwidth (low order moments of the spectral

E-mail address: nyampols@gmail.com.

http://dx.doi.org/10.1016/j.nima.2017.07.008
Received 6 April 2017; Received in revised form 30 June 2017; Accepted 6 July 2017
Available online xxxx
0168-9002/Published by Elsevier B.V.

power distribution). The spectral distribution changes when the electron beam passes through beam optics elements. As it will be shown below, one can easily find how the spectral distribution evolves along the beamline. That allows finding the change of the rms spectral parameters and eventually describing the evolution of the bunched beam.

The paper is organized as follows. In Section 2 we develop general principles for describing dynamics of modulated beams. First, we introduce the spectral distribution function describing the beam distribution in the spectral domain and find how it changes along a linear beamline. Then we introduce low order moments of the spectral distribution and find how they evolve along the beamline. Finally, we find several invariants relating spectral properties of the modulated beams which remain constant under arbitrary linear symplectic transforms. In Section 3 we describe the main methods for modulating beams and find the resulting spectral distribution function which is generated in these modulators. In Section 4 we apply developed formalism for analyzing common schemes for XFEL seeding. We demonstrate that developed theory significantly simplifies analysis and estimate the bandwidth of the output bunching in case of significant random phase noise of utilized laser pulses.

2. General description of modulated beams

Any electron beam can be described as an ensemble of electrons occupying some phase space volume. Each electron can be fully described by its position in the 6D phase space

$$\boldsymbol{\zeta}(s) = (x, p_x, y, p_y, \Delta t, -\Delta E), \tag{1}$$

where x and y are the transverse coordinates of the electron in respect to the reference trajectory, p_x and p_y are the corresponding canonical momenta, Δt is the electron arrival time to position s along the beamline, ΔE is the deviation of the particle energy from the average bunch energy.

The entire bunch as an ensemble can be described with the distribution function $f(\boldsymbol{\zeta})$ which characterizes electron density in the 6D phase space. We anticipate describing modulated electron bunch with fine scale variations in the phase space. Describing such a beam with rms quantities will requires finding high order correlations in order to capture short scale variations. It is more practical to describe modulated beams with the entire distribution function rather than with a very large number of high order moments.

2.1. Vlasov equation

Electrons interact with electro-magnetic fields which satisfy Maxwell equations. That implies that the dynamics can be described with a Hamiltonian $H(\boldsymbol{\zeta}, s)$. The evolution of the distribution function satisfies Vlasov equation which can be considered as a continuity equation in the phase space

$$\frac{df}{ds} = \partial_s f(\boldsymbol{\zeta}, s) + [f, H] = 0, \tag{2}$$

where $[f, H] = (\nabla f)^T J(\nabla H)$ is the Poison bracket, J is the unit block-diagonal antisymmetric symplectic matrix, ∇ is the 6D gradient in the phase space, and the superscript T stands for the transposition.

The Vlasov equation can be solved using the method of the characteristics. Each characteristic describes the electron trajectory in the phase space and generalizes Newton equations for an arbitrary choice of canonical variables $\boldsymbol{\zeta}$:

$$\frac{d\boldsymbol{\zeta}}{ds} = J(\nabla H). \tag{3}$$

In this paper we neglect that particles interact with each other (Hamiltonian does not depend on the distribution function). We also limit our analysis to the linear beamline optics. Such a system can be described with the Hamiltonian H, which quadratically depends on the phase space coordinate $\boldsymbol{\zeta}$. The Hamiltonian can be represented as a quadratic form defined by the symmetric matrix $\mathcal{H} = \mathcal{H}^T$

$$H(\boldsymbol{\zeta}, s) = \frac{1}{2}\boldsymbol{\zeta}^T \mathcal{H}(s)\boldsymbol{\zeta}, \tag{4}$$

$$\frac{df}{ds} = \partial_s f(\boldsymbol{\zeta}, s) + (\nabla f)^T J\mathcal{H}\boldsymbol{\zeta} = 0, \tag{5}$$

Under this assumption, Newton equations (3) become linear

$$\frac{d\boldsymbol{\zeta}}{ds} = J\mathcal{H}\boldsymbol{\zeta} \tag{6}$$

and they can be solved using, for example, Magnus expansion. The final and the initial coordinates of each particle transform linearly along the beamline through conventional symplectic transform matrix R. Then the formal solution of Vlasov equation

$$\boldsymbol{\zeta}(s) = R(s, s_0)\boldsymbol{\zeta}(s_0), \tag{7}$$

$$f(\boldsymbol{\zeta}, s) = f\left(R^{-1}(s, s_0)\boldsymbol{\zeta}, s_0\right). \tag{8}$$

This solution represents the Liouville theorem which states that the particle density is conserved along the trajectory in the phase space.

2.2. Spectral distribution function

As mentioned above, the distribution function $f(\boldsymbol{\zeta})$ of the modulated beam has small scale variations and cannot be characterized with a small number of typical parameters. However, these variations are quasi-periodic. Therefore, the Fourier spectrum of the distribution function is well localized in the spectral domain. The spectral distribution can be used then for the description of the modulated beams. This approach is similar to methods used in Optics, where laser pulses are conventionally described with their spectra rather than the actual field distribution in space. Unlike Optics, the beam is characterized with the distribution function in the 6D phase space and any component of the electron 6D position can change along the beamline. Therefore, one has to consider the 6D Fourier transform of the distribution function which introduces the spectral distribution function

$$f_{\mathbf{k}}(\mathbf{k}, s) = \int f(\boldsymbol{\zeta}, s)e^{-i\mathbf{k}^T\boldsymbol{\zeta}}d^6\boldsymbol{\zeta}. \tag{9}$$

The spectral distribution function fully describes the beam since the phase space distribution can be recovered through the inverse Fourier transform of the spectral distribution. At the same time, the spectral distribution function reflects important characteristics of the beam which are not evident from the distribution function $f(\boldsymbol{\zeta})$ in the phase space. For example, the spectral distribution function along the longitudinal axis $\hat{\mathbf{k}}_5 \equiv \hat{\mathbf{k}}_z$ is equal to the beam bunching factor, $b(k) = \int f(\boldsymbol{\zeta})e^{-ik\zeta_5}d^6\boldsymbol{\zeta} \equiv f_{\mathbf{k}}(\mathbf{k} = \hat{\mathbf{k}}_5 k)$.

The description of the modulated beams with the spectral distribution function is beneficial only if its evolution along the beamline can be described with simple enough equations. Otherwise, the model will be too complicated for practical use. Below we find the exact equation describing the change of the spectral distribution but first we show that its dynamics is simple enough. Consider a single harmonic of the spectral distribution function $f_{\mathbf{k}}(\mathbf{k}, s_0) = \delta(\mathbf{k} - \mathbf{k}')$ which corresponds to the distribution function $f(\boldsymbol{\zeta}, s_0) \propto \exp(i\mathbf{k}'^T\boldsymbol{\zeta})$. The phase of the modulation $\phi = \mathbf{k}^T\boldsymbol{\zeta}$ linearly depends on the phase space coordinate $\boldsymbol{\zeta}$. Therefore, the phase of the modulation remains linear under any linear transform of the phase space $\boldsymbol{\zeta} \to R\boldsymbol{\zeta}$, which is the case of the linear beamline optics. Therefore, a monochromatic modulation transforms into another monochromatic modulation with a different wavevector, $\mathbf{k}' \to \mathbf{k}''$. As a result, different harmonics of the spectral distribution do not mix with each other in a linear beamline and spectral distribution function is self-similar along the beamline. This property indicates that the equation describing evolution of the spectral distribution function should be simple enough.

We find the precise equation describing the dynamics of the spectral distribution function by taking the Fourier transform of the Vlasov

Please cite this article in press as: N.A. Yampolsky, Dynamics of modulated beams in spectral domain, Nuclear Inst. and Methods in Physics Research, A (2017), http://dx.doi.org/10.1016/j.nima.2017.07.008.

equation (2) and assuming the quadratic form of the Hamiltonian described with Eq. (4). Using equality $\mathrm{tr}(J\mathcal{H}) = 0$ one can derive the following equation after some straightforward algebra

$$\frac{df_{\mathbf{k}}}{ds} = \partial_s f_{\mathbf{k}} + [f_{\mathbf{k}}, H_{\mathbf{k}}]_{\mathbf{k}} = \\ = \partial_s f_{\mathbf{k}} + (\nabla_{\mathbf{k}} f_{\mathbf{k}})^T \mathcal{H} J \mathbf{k} = 0, \tag{10}$$

$$H_{\mathbf{k}}(\mathbf{k}, s) = -\frac{1}{2}\mathbf{k}^T J \mathcal{H}(s) J \mathbf{k}. \tag{11}$$

This equation has exactly the same form as the original Vlasov equation (5) and can be interpreted then as the Vlasov equation for the spectral distribution function. The dynamics of the spectral distribution function is symplectic and it is fully described with the Hamiltonian $H_{\mathbf{k}}(\mathbf{k}, s)$ defined in Eq. (11).

According to the Liouville theorem, the spectral distribution function does not change along the trajectory in $\mathbf{k}$ space, and therefore, it can be considered as an ensemble of non-interacting quasi-particles. Each quasi-particle represents one spectral harmonic of the spectral distribution. These quasi-particles do not vanish and are not created in time, they do not interact or mix with each other, and their entire dynamics manifests as motion along trajectories in the $\mathbf{k}$ space. The only fundamental difference between the descriptions in the phase space and the spectral domain is that the spectral distribution function can be complex unlike the phase space distribution function which is real and positive.

Each harmonic of the spectral distribution function remains as a single harmonic along the linear beamline. This property indicates that the linear beam optics cannot be used for generating high order harmonics of modulation. This observation does not contradict performance of the high gain harmonic generation (HGHG) [9] or echo-enabled harmonic generation (EEHG) [10] schemes. As it will be shown in Section 3.2 that high order harmonics are generated in the modulator in which the phase space of the beam transforms nonlinearly. The following chicanes do not create additional harmonics in the spectral domain but only transform the imposed modulation into the longitudinal bunching.

In order to solve the spectral Vlasov equation (10) we note that it is a hyperbolic partial differential equation, similar to the conventional Vlasov equation (5). Therefore, it can be solved using the method of the characteristics. Each spectral component remains constant along the following trajectory in $\mathbf{k}$ space

$$\frac{d\mathbf{k}}{ds} = \mathcal{H} J \mathbf{k}. \tag{12}$$

The characteristics equation (12) for each spectral harmonic is similar to characteristics equation (6) describing the trajectory of each individual particle. Therefore, these linear equations can be solved using the same techniques. At the same time, these two solutions are related to each other since the corresponding equations contain the same matrices. One can note that two arbitrary solutions of Eqs. (6) and (12) do not evolve independently and their product is invariant along the beamline

$$\frac{d(\mathbf{k}^T \boldsymbol{\zeta})}{ds} = 0, \tag{13}$$

Using the solution for the particle trajectory (7) and noticing that the relation (13) holds for any arbitrary initial particle position $\boldsymbol{\zeta}(s_0)$, one finds the solution for the spectral characteristics

$$\mathbf{k}(s) = R^{-T}(s, s_0)\mathbf{k}(s_0), \tag{14}$$

where the superscript $(.)^{-T}$ denotes the inverse transposition of a matrix (these two operators commute with each other). This relation describes the change of the wavevector for each harmonic. The solution of the spectral Vlasov equation (10) reads then as

$$f_{\mathbf{k}}(\mathbf{k}, s) = f_{\mathbf{k}}(R^T(s, s_0)\mathbf{k}, s_0). \tag{15}$$

2.3. Spectral averages

The beam is fully described with its spectral distribution function $f_{\mathbf{k}}(\mathbf{k}, s)$. Depending on the circumstances, few average parameters of the spectral distribution function may suffice to characterize its main features. We introduce the spectral averaging of some variable $g(\mathbf{k})$ as

$$\overline{g(\mathbf{k})}(s) = \frac{\int g(\mathbf{k})|f_{\mathbf{k}}(\mathbf{k}, s)|^2 d^6\mathbf{k}}{\int |f_{\mathbf{k}}(\mathbf{k}, s)|^2 d^6\mathbf{k}}. \tag{16}$$

Note that we use overline notation $\bar{\cdot}$ to characterize the spectral averages in order to distinguish them from the averages in the phase space domain defined as $\langle\cdot\rangle$. The denominator in Eq. (16) remains constant in the linear beamlines and serves as the normalization factor so that the quantity itself and its spectral average have the same dimensions.

The spectral distribution function is localized in some region of the spectral domain in case of a narrowband modulation . Such a distribution can be well characterized with a few low order moments. We introduce the spectral average wavevector of the modulation $\bar{\mathbf{k}}(s)$ and the second order spectral correlation matrix

$$B(s) = \overline{(\mathbf{k} - \bar{\mathbf{k}})(\mathbf{k} - \bar{\mathbf{k}})^T}. \tag{17}$$

This matrix describes the rms spreads of the spectral distribution function $f_{\mathbf{k}}(\mathbf{k}, s)$. The diagonal elements describe the modulation bandwidths along the corresponding axes. Therefore, we call the matrix B as the "bandwidth matrix". The bandwidth matrix defines the rms ellipsoid in the spectral domain similar to the rms envelope ellipsoid defined by the beam matrix $\Sigma = \langle\boldsymbol{\zeta}\boldsymbol{\zeta}^T\rangle$. This rms bandwidth ellipsoid qualitatively shows noise distribution along different dimensions.

In some cases the spectral distribution function $f_{\mathbf{k}}(\mathbf{k}, s)$ can be localized in several well separated regions of the spectral domain, *e.g.* the spectrum of the beam modulated with the laser pulse consists of several localized harmonics as will be shown in Section 3.2. The Vlasov equation (10) for the spectral distribution function states that different trajectories in the spectral domain do not cross which does not allow well separated spectral domains mixing with each other. In this case the spectral average quantities can be introduced for each localized domain individually.

Using Eq. (15) describing the change of the spectral distribution function along the beamline, one can easily find transforms of the spectral averages

$$\bar{\mathbf{k}}(s) = R^{-T}(s, s_0)\bar{\mathbf{k}}(s_0), \tag{18}$$

$$B(s) = R^{-T}(s, s_0)B(s_0)R^{-1}(s, s_0). \tag{19}$$

The wavevector of the modulation changes linearly along the beamline. One can consider the setup in which the wavelength of the initial modulation is scaled while its orientation in the 6D spectral domain is fixed. Linear transform of the modulation wavevector along the beamline indicates the same scaling of the output modulation wavelength. This property can be used while designing the masked dogleg [17] or the Emittance EXchanger (EEX) [15] schemes to generate bunches with different spatial spacing. Different spacing between bunches can be achieved if several masks with different spacing between the slits are used. At the same time, the optics required to transform the imposed modulation into the longitudinal bunching remains the same for different masks.

The bandwidth matrix $B(s)$ transforms exactly in the same way as the inverse beam matrix Σ^{-1},

$$\Sigma(s) \equiv \langle\boldsymbol{\zeta}\boldsymbol{\zeta}^T\rangle = R(s, s_0)\Sigma(s_0)R^T(s, s_0). \tag{20}$$

This property becomes evident if one considers unmodulated beam with some envelope. In this case the average modulation wavenumber is close to zero and the bandwidth matrix describes the rms wavevector spread of the spectral distribution which is inversely proportional to the rms beam sizes. Moreover, if one considers the beam with the 6D Gaussian distribution, $f \propto \exp(-\boldsymbol{\zeta}^T \Sigma^{-1} \boldsymbol{\zeta}/2)$, then the bandwidth matrix is related

Please cite this article in press as: N.A. Yampolsky, Dynamics of modulated beams in spectral domain, Nuclear Inst. and Methods in Physics Research, A (2017), http://dx.doi.org/10.1016/j.nima.2017.07.008.

to the rms beam matrix as $B = \Sigma^{-1}/2$ (this property can be proved through direct calculation of integrals in Eqs. (9) and (16) by transforming integration variables according to Eq. (A.1) which diagonalizes the matrices). This relation also holds if an arbitrary monochromatic modulation is imposed on the beam with the 6D Gaussian envelope since such a modulation changes the average wavevector but does not affect the bandwidth matrix. At the same time, if the imposed modulation is not monochromatic and has some bandwidth due to noise, then the resulting bandwidth matrix deviates from $\Sigma^{-1}/2$. This example shows that describing modulated beam with the bandwidth matrix is useful only in the presence of significant noise when $\|I - 2B\Sigma\| \gg \|I\|$. Otherwise, the modulation can be considered monochromatic and it is more convenient to describe the beam with its phase space envelope and a single wavevector of the modulation. Introducing the bandwidth matrix for the monochromatic modulation is not feasible since it is strongly related to the beam matrix Σ and does not provide additional information.

Note that the bandwidth matrix is a useful concept for describing the beam quality even if the beam is not modulated. While the rms beam matrix Σ describes large scale features of the beam such as its rms sizes, energy, and angular spreads, the bandwidth matrix B describes small-scale fluctuations in the distribution function. Therefore, the bandwidth matrix describes the beam homogeneity and it is more homogeneous at smaller values of $\|I - 2B\Sigma\|$.

The modulation wavevector and the bunch envelope transform independently from each other. Identical envelopes transform in the same way regardless what kind of modulation is imposed on the bunch. Alternatively, identical modulations imposed on bunches with different envelopes also transform identically. This property significantly simplifies the task of designing beam buncher since it can be designed independently from the rest of the beamline. This beamline section should solve the problem of transforming imposed modulations into the required modulations and this optics does not depend on rms beam quantities such as its sizes and emittances. Once designed, this block can be attached to any accelerator and it will perform equally in any regime of the machine.

2.4. Modulation invariants

The bandwidth matrix is a positively defined symmetric matrix which transforms along the beamline through the symplectic matrix $R^T J R = J$. This transform is similar to the transform (20) of the beam rms matrix Σ. Therefore, the invariants which hold for the beam matrix [18] are also applicable to the bandwidth matrix

$$\det(B) = inv, \tag{21}$$

$$\mathrm{tr}(BJ)^{2n} = inv, \quad n = 1, 2, \ldots dim(B)/2. \tag{22}$$

These invariants can be used to introduce parameters similar to the eigen-emittances for the beam envelope [18].

Other than that, one can note that the change of the spectral averages is fully described with the transform matrix R. This is not surprising since the transform matrix defines the mapping of each particle in the phase space, and therefore, describes the entire beam dynamics. Therefore, spectral averages do not transform fully independently from the beam rms quantities. Combining Eqs. (18) and (20) one can easily find the following scalar quantity which remains constant along arbitrary linear beamline

$$\bar{\mathbf{k}}^T(s)\Sigma(s)\bar{\mathbf{k}}(s) = inv. \tag{23}$$

This quantity can be interpreted as the overall phase of the modulation across the bunch envelope. To illustrate this invariant one may consider imposing longitudinal bunching on the beam and its compression in the following beamline. In this case, the number of modulation periods within the rms beam length remains constant during compression, *i.e.* the overall phase of the modulation is invariant.

Additional invariants can be found by taking into account that the transform matrix R describes Hamiltonian dynamics and, therefore, is symplectic. Using Eqs. (18), (20), one can construct the following invariants

$$\bar{\mathbf{k}}^T J(\Sigma^{-1}J)^{2n+1}\bar{\mathbf{k}} \equiv \bar{\mathbf{k}}^T (J\Sigma^{-1})^{2n+1} J\bar{\mathbf{k}} = inv,$$
$$n = 1, 2, \ldots dim(\Sigma)/2. \tag{24}$$

There is an infinite number of invariants but the number of functionally independent ones is equal to 3 in general case. Moreover, these invariants are not functionally independent from Eq. (23).

Invariants (24) can be understood using the concept of the eigen-emittances as described in Appendix. They state that the overall phase of modulation across each eigen-phase plane is preserved. This property can guide attempts for beam bunching using transverse masking. It is of particular practical interest to consider beams which eigen-emittances are recovered as x-, y-, and z- emittances since this scenario corresponds to the brightest beam with the fixed phase space volume. Transverse masking modulates the beam along x which implies modulation in a single eigen-phase plane in case of uncorrelated beam. According to invariants (24) the modulation imposed in one eigen-phase plane remains in the same eigen-phase plane along the beamline. This indicates that the downstream optics should swap (x, p_x) and $(\Delta t, -\Delta E)$ phase planes if one wishes to achieve an uncorrelated beam with longitudinal modulation. Therefore, one should use the EEX optics [19] to achieve this goal. Otherwise, the modulation can be smeared out at significantly large emittances as it was reported in Ref. [17].

The bandwidth matrix transforms exactly in the same way as the inverse rms beam matrix. Therefore, the invariants involving the bandwidth matrix are similar to invariants (23) and (24) found for the beam matrix

$$\bar{\mathbf{k}}^T B^{-1}\bar{\mathbf{k}} = inv, \tag{25}$$

$$\bar{\mathbf{k}}^T J(BJ)^{2n+1}\bar{\mathbf{k}} = inv, \quad n = 1, 2, 3. \tag{26}$$

Invariant described with Eq. (25) can be interpreted as the conservation of the relative bandwidth $\delta k/k$ along the beamline. In case of the monochromatic modulation, the invariant (25) is exactly the same as invariant (23) since the bandwidth matrix is proportional to the inverse beam matrix.

3. Beam modulators

In this section we describe ways to impose modulations on the beam. Currently, there are two known ways for modulating the beams, namely the transverse masking and imposing spatially dependent energy modulation.

3.1. Transverse masking

The beam can be modified by passing it through the mask. The mask serves as a filter which either absorbs some particles or strongly changes their phase space coordinates so that they can be filtered out downstream the beamline. Significant change of the phase space coordinates for some group of particles while keeping intact the rest of the beam requires presence of non-Hamiltonian forces such as incoherent damping, scattering, ionization, *etc*. The simplest mask can be envisioned as a perforated foil installed transversally to the bunch propagation. Electrons passing through the foil strongly scatter and are lost downstream while electrons passing through the opening remain intact. These masks modify the bunch transversally and they are widely used in accelerator technology. Modifying the distribution function along other phase space coordinates would require differentiation of particles based on their position in the phase space: different ionization cross-section at different energies, triggering interaction externally at a certain time, *etc*.

Please cite this article in press as: N.A. Yampolsky, Dynamics of modulated beams in spectral domain, Nuclear Inst. and Methods in Physics Research, A (2017), http://dx.doi.org/10.1016/j.nima.2017.07.008.

Without addressing particular physical mechanism of masking, we consider that the bunch distribution function can be changed by the mask as

$$f(\boldsymbol{\zeta}) = f^0(\boldsymbol{\zeta})M(\boldsymbol{\zeta}), \tag{27}$$

where f^0 is the distribution function of the bunch before the mask and M is the mask imprint. The spectral distribution function of the resulting beam $f_{\mathbf{k}}(\mathbf{k})$ can be presented as a convolution of the initial and the mask spectral distribution functions $f^0_{\mathbf{k}}(\mathbf{k})$ and $M_{\mathbf{k}}(\mathbf{k})$, respectively

$$f_{\mathbf{k}}(\mathbf{k}) = f^0_{\mathbf{k}} * M_{\mathbf{k}} = \int f^0_{\mathbf{k}}(\mathbf{k}')M_{\mathbf{k}}(\mathbf{k}-\mathbf{k}')d^6\mathbf{k}', \tag{28}$$

This equation provides a semi-qualitative description for the modulated beam spectral properties. We consider both the beam and the mask spectra to be well-localized. If their bandwidths can be neglected *i.e.* their spectra can be well approximated with δ-functions, the wavevector of the resulting modulation can be approximated as

$$\bar{\mathbf{k}}[f_{\mathbf{k}}] \approx \bar{\mathbf{k}}[f^0_{\mathbf{k}}] + \bar{\mathbf{k}}[M_{\mathbf{k}}]. \tag{29}$$

Note that using the perforated foil as a mask modulates the beam in the transverse plane. For example, a set of wires aligned along y and placed periodically along x shifts the average wavevector of modulation along k_x.

Taking into account finite bandwidths of the initial beam and the mask results in the finite bandwidth of the resulted modulation. In some cases (Gaussian or uncorrelated spectra) the spectral bandwidths add in quadrature to each other. In general case, the bandwidth of the resulting beam cannot be related to the bandwidths of the initial beam and the mask without knowledge about the spectral distribution functions. It can be just noted that if one of the bandwidth is much larger then another, then the bandwidth of the convolution is approximately equal to the largest one.

3.2. Energy modulation with laser pulse

In this scheme the beam acquires the spatially dependent energy modulation [9]. Such a modulation can be imposed through resonant interaction with a laser pulse inside the undulator. Interaction of the laser pulse with electron beam results in the change of the particle energy $E \to E - \delta E \sin\varphi(z)$. The resulting beam distribution function $f(z,E)$ relates to the distribution function of the unperturbed beam $f^0(z,E)$ as

$$f(z,E) = f^0(z, E + \delta E \sin\varphi(z)), \tag{30}$$

where for simplicity of description we omitted transverse variables.

Ideally, the laser is considered to be monochromatic, *i.e.* $\varphi(z) = kz$. In order to extend our analysis we consider that the laser has finite bandwidth caused by random fluctuations in its phase (and consider the laser amplitude to be spatially uniform). As a result, the laser phase consists of a linear term and a random perturbation. In order to characterize such a laser, we introduce its spectral distribution function

$$\boldsymbol{\Phi}_k(k) = \int e^{i\varphi(z)-ikz}dz. \tag{31}$$

The average laser wavelength and bandwidth are defined then as

$$\bar{k}_{laser} = \bar{k}[\boldsymbol{\Phi}_k] \equiv \frac{\int k|\boldsymbol{\Phi}_k(k)|dk}{\int|\boldsymbol{\Phi}_k(k)|dk} \tag{32}$$

$$\overline{\delta k^2}_{laser} = \overline{(k-\bar{k}_{laser})^2}[\boldsymbol{\Phi}_k]. \tag{33}$$

The spectral distribution function of the modulated beam described with Eq. (30) can be related to the spectral distribution functions of the initial beam $f^0_{\mathbf{k}}$ and the spectral distribution of the laser phase $\boldsymbol{\Phi}_k$. After some straightforward algebra one can find that the beam spectrum consists of the infinite number of harmonics

$$f_{\mathbf{k}}(k_z,k_E) = \sum_{n=-\infty}^{\infty} f^{(n)}_{\mathbf{k}}(k_z,k_E) = \\ = \sum_{n=-\infty}^{\infty} J_n(|k_E\delta E|)f^0_{\mathbf{k}}(k_z,k_E) * \underbrace{\boldsymbol{\Phi}_k(k_z) * \ldots * \boldsymbol{\Phi}_k(k_z)}_{n}, \tag{34}$$

where J_n is the nth order Bessel function. The schematics of the spectrum is presented in Fig. 1. On that plot the beam envelope was considered to be uniform along k_E, which corresponds to the monoenergetic beam. In reality, the beam has an energy spread and the corresponding spectral distribution of the unperturbed beam $f^0_{\mathbf{k}}$ has some finite bandwidth along k_E which is shown as a shaded area. The spike in the vicinity of $k_E = 0, k_z = 0$ corresponds to the Fourier transform of the modulated beam envelope. It significantly differs from the original beam envelope if the amplitude of the energy modulation is larger than the energy spread of the beam.

The form of the spectral distribution function described with Eq. (34) determines the main parameters of the modulation spectrum. The spectrum consists of the infinite number of harmonics. The spectral distribution function along the longitudinal wavenumber k_z is described with n times convolution of the laser spectral distribution $\boldsymbol{\Phi}_k(k_z)$. As discussed in Section 3.1 the spectral properties of such a distribution cannot be found in general case. However, if one assumes that the laser phase noise is stationary and Gaussian (the laser spectrum is δ-correlated which can be assumed if the laser bandwidth is mainly defined by the noise rather than its envelope and the statistics of the noise is Gaussian) then the spectral properties of the beam modulation can be found as

$$\bar{k}_z[f^{(n)}_{\mathbf{k}}] = \bar{k}_z[f^0_{\mathbf{k}}] + n\bar{k}_{laser}, \tag{35}$$

$$B_{k_z,k_z}[f^{(n)}_{\mathbf{k}}] = B_{k_z,k_z}[f^0_{\mathbf{k}}] + |n|\overline{\delta k^2}_{laser}, \tag{36}$$

i.e. the carrier frequency scales linearly with the harmonic number and the bandwidths add in quadrature. At the same time, the modulation bandwidth increases much faster with the harmonic number if the laser phase noise is not random . For example, the modulation bandwidth scales linearly with harmonic number, $B_{k_z,k_z} = B_{k_z,k_z}[f^0_{\mathbf{k}}] + n^2\overline{\delta k^2}_{laser}$, if one considers a chirped laser pulse . This effect can be proved by expressing the nth order convolution as $\boldsymbol{\Phi}_k(k_z) * \ldots * \boldsymbol{\Phi}_k(k_z) = \int e^{in\varphi(z)-ik_zz}dz$, which indicates a linear scaling of the chirp with the harmonic number.

Unlike the longitudinal spectral distribution along k_z, the energy spectral distribution along k_E is equal to the product of the initial beam spectrum and the modulation spectrum which is equal to the Bessel functions. The product of these two spectra does not vanish as long as both distributions are significant in the same domain. The schematics of the beam spectrum resulting from its energy modulation with a laser is shown in Fig. 1. The dashed area schematically shows the energy bandwidth caused by the initial beam envelope (which is on the order of the inverse energy spread of the original beam). The harmonics having significant amplitude within that bandwidth are present in the spectrum and high order harmonics outside the bandwidth are heavily suppressed.

In order to find the energy wavenumber $(k^{(n)}_E)_{\max}$ which maximizes each harmonic one needs to maximize the spectral distribution function

$$\frac{\partial}{\partial_{k_E}}\left(J_n(|k_E\delta E|)f^0_{\mathbf{k}}(k_z,k_E)\right)\Big|_{(k^{(n)}_E)_{\max}} = 0. \tag{37}$$

This equation can be solved assuming certain beam energy distribution, otherwise the problem cannot be tracked analytically. Typically the beam is assumed to have the Gaussian energy distribution (so as its energy spectrum) [9,10,20]. The main features can be recovered considering the beam energy bandwidth to be very large, *i.e.* the beam energy spread is considered to be small. Then the maximum of nth harmonic is not affected by the energy bandwidth of the original beam

Please cite this article in press as: N.A. Yampolsky, Dynamics of modulated beams in spectral domain, Nuclear Inst. and Methods in Physics Research, A (2017), http://dx.doi.org/10.1016/j.nima.2017.07.008.

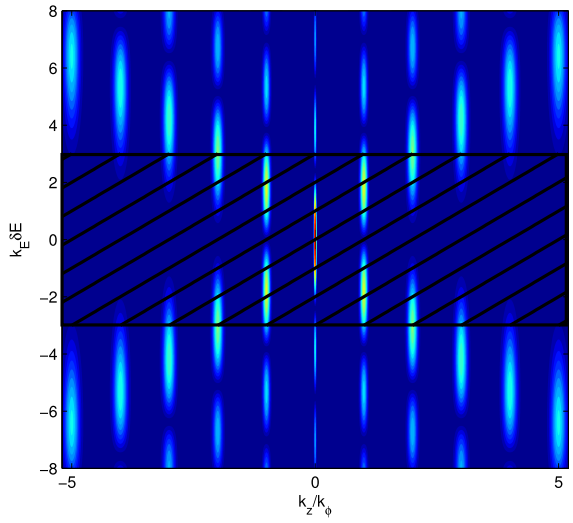

Fig. 1. (Color online) Spectrum of modulation produced by the spatial variation of the beam energy. Dashed area schematically shows the energy bandwidth of the original beam.

envelope and it is located at $(k_E^{(n)})_{\max} \approx \mu_{n1}/\delta E$, where μ_{n1} is the first maximum of nth order Bessel function, $J_n'(\mu_{n1}) = 0$. Therefore, the modulation is not heavily suppressed by the finite beam energy spread if the modulation is significantly large $(k_E^{(n)})_{\max} \lesssim (B_{k_E,k_E}[f_{\mathbf{k}}^0])^{1/2}$ or $\delta E \gtrsim \mu_{n1}\sigma_E \sim n\sigma_E$, where σ_E is the rms energy spread of the original beam envelope. Note that this condition is harder to satisfy for modulations at higher harmonics which agrees with the scaling of the HGHG scheme [9].

The energy bandwidth of the resulting distribution (B_{k_E,k_E} element of the bandwidth matrix) is not well defined since the spectral energy distribution consists of several spikes which are described with oscillating Bessel function. One cannot consider them individually since they are not well separated in the spectral domain. However, one can characterize the spectral distribution bandwidth with its curvature at the maximum, $B_{k_E,k_E} \sim -0.5 f_{\mathbf{k}}(k_z,k_E)/\left(\partial^2_{k_E,k_E} f_{\mathbf{k}}(k_z,k_E)\right)$. For low order harmonics, $\mu_{n1} \lesssim \delta E/\sigma_E$, and large enough modulations, $\delta E \gg \sigma_E$, one finds

$$B^{(n)}_{k_E,k_E} \approx -\frac{1}{2}\left.\frac{f^{(n)}_{\mathbf{k}}(k_z,k_E)}{\partial^2_{k_E,k_E} f^{(n)}_{\mathbf{k}}(k_z,k_E)}\right|_{(k_E^{(n)})_{\max}} = \\ = \frac{\mu_{n1}^2}{\mu_{n1}^2 - n^2}\frac{1}{(\delta E)^2} \sim \frac{0.618 n^{2/3}}{(\delta E)^2}, \quad \begin{matrix} n \gg 1 \\ n \lesssim \delta E/\sigma_E. \end{matrix} \tag{38}$$

Eq. (34) shows that the non-diagonal terms of the resulting bandwidth matrix $B_{k_z,k_E} = B_{k_E,k_z}$ are equal to zero if these terms were zero for the original beam envelope before the modulation was applied. This approximation is typically valid for beams without energy chirp. Then the bandwidth matrix for each harmonic can be approximated as

$$B[f^{(n)}_{\mathbf{k}}] = \begin{pmatrix} B_{k_z,k_z}[f^0_{\mathbf{k}}] + |n|\overline{\delta k^2}_{laser} & 0 \\ 0 & \dfrac{\mu_{n1}^2}{\mu_{n1}^2 - n^2}\dfrac{1}{(\delta E)^2} \end{pmatrix}. \tag{39}$$

Note that this expression describes the characteristic spectral bandwidth rather than the exact spectral average value. Therefore, transforms and invariants for the bandwidth matrix found in Sections 2.3 and 2.4 should be used with caution.

4. Transforms of beam modulation in various schemes

In this section we illustrate the developed formalism describing evolution of the modulated beams in the spectral domain. We consider common schemes for the XFEL seeding which rely on the beam modulation by a laser and transforming the imposed modulation into the longitudinal bunching at small wavelengths. As described in Section 3.2 the relevant beam dynamics occurs in the longitudinal phase space, $\boldsymbol{\zeta} = (t, -\Delta E)^T$. Therefore, we limit our analysis to the 2D distribution function in the longitudinal phase space and its spectrum. The application of the developed technique to some cases in which dynamics in the longitudinal and the transverse phases planes is mixed is demonstrated in Ref. [21]

Conventional schemes for creating the beam bunching from the laser-induced energy modulation rely on two types of beam optics elements, namely chicanes and RF cavities introducing the energy chirp. These elements transform the wavevector of the modulation in the 2D spectral domain as $\mathbf{k} = R^{-T}\mathbf{k}^0$, where the transform matrices for these elements have the following form:

$$R_{\text{chicane}} = \begin{pmatrix} 1 & \xi \\ 0 & 1 \end{pmatrix} \qquad R_{\text{cavity}} = \begin{pmatrix} 1 & 0 \\ \alpha & 1 \end{pmatrix}. \tag{40}$$

As a result, the wavevector of the modulation transforms by these elements as

$$\begin{pmatrix} k_z \\ k_E \end{pmatrix} = R^{-T}_{\text{chicane}} \begin{pmatrix} k^0_z \\ k^0_E \end{pmatrix} = \begin{pmatrix} k^0_z \\ k^0_E - \xi k^0_z \end{pmatrix}, \tag{41}$$

$$\begin{pmatrix} k_z \\ k_E \end{pmatrix} = R^{-T}_{\text{cavity}} \begin{pmatrix} k^0_z \\ k^0_E \end{pmatrix} = \begin{pmatrix} k^0_z - \alpha k^0_E \\ k^0_E \end{pmatrix}. \tag{42}$$

It is easy to follow these transforms in the 2D spectral plane as will be shown in Figs. 2 and 3 in the next section. Any given scheme can be represented with a diagram which shows trajectory of the modulation wavenumber between the initial and final values. The following notations on these diagrams will be used:

- Consider the laser induced modulation imposed on the beam. This modulation has spectral distribution function which peaks at the wavevector $\mathbf{k} = (2\pi n/\lambda, (k_E^{(n)})_{\max})^T$, where λ is the laser wavelength and $(k_E^{(n)})_{\max}$ can be found from Eq. (37). We will focus on the evolution of the vicinity of this spectral component since it has the largest harmonic current and we will mark this wavevector with a cross.
- Each beam optics element transforms the modulation wavevector according to Eqs. (41) and (42). The modulation wavevector changes its k_E component when the beam passes through some chicane and it changes k_z component when the beam passes through some RF cavity. We will illustrate these transforms with arrows starting from the initial and ending at the final wavevector of the modulations Note that chicanes and cavities will be represented as arrows parallel to the spectral space axes. Also note that chicanes are typically considered to have positive dispersion $\xi > 0$. Therefore, they will be represented with downward arrows in the right-hand side of the diagram (positive harmonic number, $k_z > 0$) and upward arrows in the left-hand side of the diagram (negative harmonic numbers $k_z < 0$).
- Some schemes require imposing laser-induced modulation several times along the beamline. As discussed in Section 3.2 the modulation does not vanish only in the vicinity of k_E where both the beam envelope and the modulation have significant spectral distributions. In these schemes the harmonic current imposed by the first laser and transformed in the beamline can serve as an envelope in the following modulator. We will mark this mechanism by a dashed arrow parallel to k_z axis (modulation by the second laser does not vanish only in the vicinity of k_E of already existing modulations). Not that this arrow refers to the nonlinear modification of the beam spectrum unlike solid arrows which refer to the linear transforms in which different spectral harmonics do not mix with each other.

All the schemes considered below are designed to transform the initial modulation into the longitudinal bunching. Therefore, the linear beamline optics is designed to transform the wavevector of the imposed modulation into $\mathbf{k} = (k_z, 0)^T$, *i.e.* to eliminate any the energy modulation.

Please cite this article in press as: N.A. Yampolsky, Dynamics of modulated beams in spectral domain, Nuclear Inst. and Methods in Physics Research, A (2017), http://dx.doi.org/10.1016/j.nima.2017.07.008.

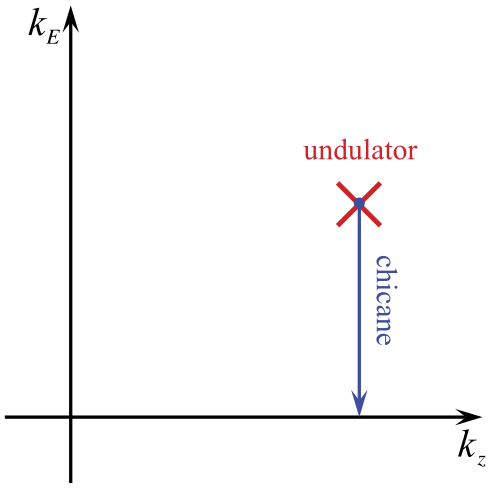

Fig. 2. (Color online) Schematics for the modulation transform in the HGHG scheme.

4.1. High gain harmonic generation (HGHG)

In this scheme the energy modulation imposed by the laser pulse in a short undulator section is linearly transformed by the following chicane [9]. The schematics for the transform of the modulation wavevector is presented in Fig. 2. Considering the final modulation to be longitudinal bunching (*i.e.* $k_E = 0$), one can easily recover the chicane strength which maximizes the output bunching factor

$$\xi = \frac{(k_E^{(n)})_{\max}}{2\pi n/\lambda} \sim \frac{\lambda}{2\pi\delta E}, \quad \text{for } \frac{\delta E}{\sigma_E} \gg n \gg 1. \tag{43}$$

As discussed in Section 3.2 and illustrated in Fig. 1, the modulation at high harmonics is heavily suppressed because the $(k_E^{(n)})_{\max} \sim n/\delta E$ increases with the harmonic number and eventually does not fit within the energy bandwidth of the beam envelope. That results in the reduced amplitude of the spectral distribution as follows from Eq. (34). The largest harmonic number which is present in the beam spectrum can be estimated as $n_{\max} \sim \delta E/\sigma_E$.

Fig. 3 shows the evolution of the spectral distribution function along the HGHG beamline. The original beam (plot (3(a)) is not modulated and its spectrum is localized at $k_z \approx 0$. Plot (3(b)) shows the spectral distribution of the beam after it has been modulated by the laser. A number of temporal harmonics can be observed and the highest observable harmonic is consistent with the estimate $n_{\max} \sim \delta E/\sigma_E = 5$. The red cross in plot 3 indicates the maximum of 5th harmonic which is designed to transform into the longitudinal bunching at the end of the HGHG beamline. Plot (3(c)) shows the spectral distribution after the chicane. The red arrow shows the transform of the 5th harmonic by the chicane and it is recovered as the longitudinal bunching, *i.e.* $k_E = 0$.

Tracking the evolution of the spectral distribution function along the beamline through the beamline as show in Fig. 3 provides a comprehensive understanding about the beam dynamics. However, the plot becomes very crowded if a large number of harmonics is present. It is particularly problematic tracking dynamics if several undulators are present since each modulator multiplies the harmonics. The schematics shown in Fig. 2 tracks only the location of a chosen harmonic and represents a simple visualization of the modulation transform through the beamline.

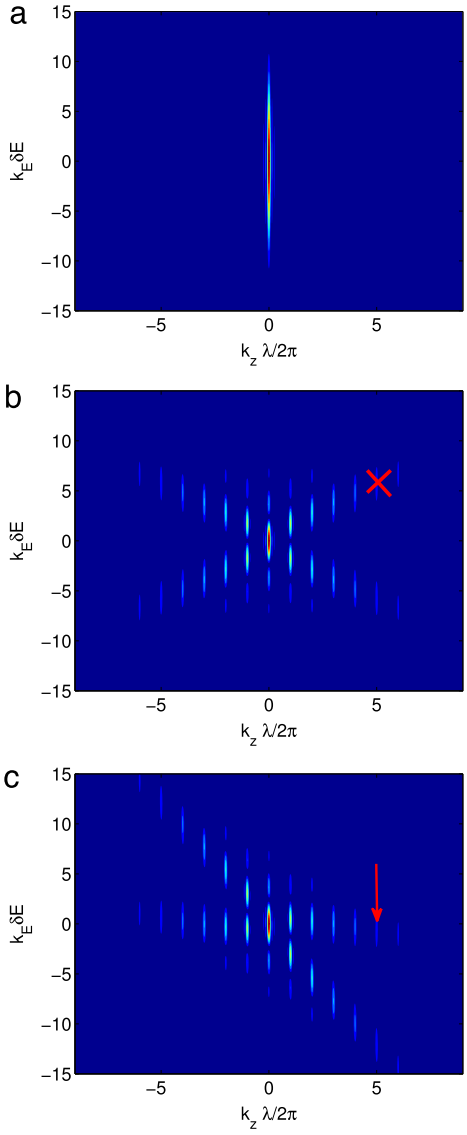

Fig. 3. (Color online) Evolution of the spectral distribution in the HGHG scheme with $\delta E = 5\sigma_E$. (a) The spectral distribution of the initial beam. (b) The spectral distribution after the undulator. (c) The spectral distribution after the chicane. Red cross in plot (b) shows the appearance of the 5th harmonic and red arrow in plot (c) shows its transform into the longitudinal bunching.

The bandwidth matrix can be found using Eq. (39). Assuming that the bandwidth is mainly determined by the laser phase noise, one obtains the following bandwidth matrix of the modulation at the end of the HGHG scheme

$$B_{\text{HGHG}}^{(n)} = R_{\text{chicane}}^{-T} B[f_{\mathbf{k}}^{(n)}] R_{\text{chicane}}^{-1} = \begin{pmatrix} n\overline{\delta k^2}_{laser} & -\xi n\overline{\delta k^2}_{laser} \\ -\xi n\overline{\delta k^2}_{laser} & \frac{\mu_{n1}^2}{\mu_{n1}^2 - n^2}\frac{1}{(\delta E)^2} + \xi^2 n\overline{\delta k^2}_{laser} \end{pmatrix}. \tag{44}$$

The bandwidth matrix transformed by the chicane is not diagonal anymore. This indicates that the rms bandwidth ellipse is not aligned along k_z and k_E axes. Therefore, the extent of this rms bandwidth ellipse along k_z axis (which defines the bunching bandwidth) can be significantly smaller than the B_{k_z,k_z} bandwidth matrix element. The bandwidth of the resulting bunching can be found in the limit of a large

Please cite this article in press as: N.A. Yampolsky, Dynamics of modulated beams in spectral domain, Nuclear Inst. and Methods in Physics Research, A (2017), http://dx.doi.org/10.1016/j.nima.2017.07.008.

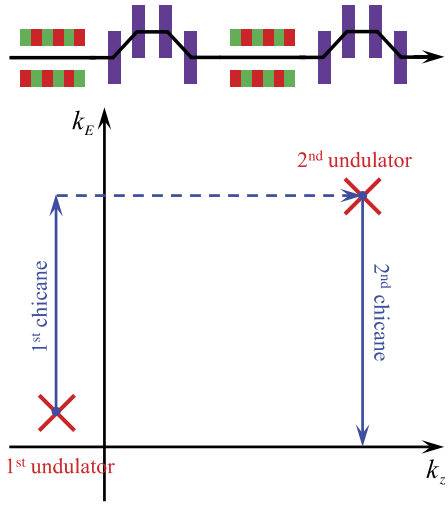

Fig. 4. (Color online) Schematics for the modulation transform in the EEHG scheme.

harmonic number, $n \gg 1, \mu_{n1} \approx n + 0.81n^{1/3}$

$$\left(\frac{\overline{\delta k^2}}{\bar{k}^2}\right)^{(n)}_{\text{HGHG}} = \frac{1}{(n\bar{k}_{laser}, 0)\left(B^{(n)}_{\text{HGHG}}\right)^{-1}(n\bar{k}_{laser}, 0)^T} = \frac{1}{n}\frac{\overline{\delta k^2}_{laser}}{\bar{k}^2_{laser}}\left(1 + 3.23n^{4/3}\frac{\overline{\delta k^2}_{laser}}{\bar{k}^2_{laser}}\right)^{-1}. \quad (45)$$

This estimate indicates that the relative bunching bandwidth at nth harmonic is roughly $\sqrt{n}$ times smaller than the relative bandwidth of the laser with δ-correlated phase noise. The second term in Eq. (45) shows additional noise filtering due to the presence of the chicane. However, this term is close to unity for low order harmonics ($n \sim 5$) and relatively narrowband lasers, $\sqrt{\overline{\delta k^2}_{laser}/\bar{k}^2_{laser}} \sim 10^{-4}$.

4.2. Echo enabled harmonic generation (EEHG)

As discussed in Sections 3.2 and 4.1, the main limitation on generating modulation at high harmonics of the laser wavelength comes from the limited overlap between the energy bandwidths of the beam envelope and the laser induced modulation. As illustrated in Fig. 1, the modulation at high harmonics is located at high values of $(k_E^{(n)})_{\max} \sim n/\delta E$ which eventually fall outside the energy bandwidth of the beam envelope. As a result, the amplitude of the modulation rapidly drops as indicated by Eq. (34). This drawback can be compensated by increasing the amplitude of the imposed energy modulation. Such an approach increases modulation amplitude but also results in the increased rms beam energy spread which may reduce FEL performance. Alternatively, the beam envelope can be modified in such a way that its energy bandwidth is shifted to the domain in which high order harmonics are produced. This is precisely the scenario which takes place in the EEHG scheme [10]. In this scheme the beam is first modulated with the laser pulse. The following strong chicane is used to increase the k_E component of the $n_1 = -1$ harmonic of the modulation. Then the second modulator is used and $n_1 = -1$ harmonic of the already imposed modulation serves as the beam envelope for the secondary modulation. As a result, harmonics are generated in the domain with increased k_E values, *i.e.* high order harmonics with $n_2 \gg 1$ can be generated. The schematics of the EEHG scheme is presented in Fig. 4.

The condition for the overlap of two modulations along k_E coordinate determines the first chicane strength (for the optimized performance of the EEHG scheme at a given harmonic number). The strength of the second chicane can be determined from the condition that the final modulation should be recovered as the longitudinal bunching, *i.e.* $k_E = 0$ after the second chicane. Taking these conditions simultaneously results exactly in the same equations as presented in Ref. [10]. Note that the first chicane is used to increase k_E component of the beam modulation. This process results in a strong energy modulation of the beam, *i.e.* creating energy bands within the beam envelope which are observed in simulations [10].

The resulting bunching is linearly transformed from the modulation produced in the second modulator. The energy bandwidth B_{k_E,k_E} is mostly determined by the energy bandwidth of $n_1 = -1$ harmonic generated in the first modulator for $n = n_1 + n_2 \gg 1$, $\delta E_1 \sim \delta E_2$, which follows from Eq. (38). At the same time, the spatial bandwidth of the resulting modulation B_{k_z,k_z} increases every time the laser modulation is applied. Finding the precise bandwidth matrix of the resulting modulation is complicated since the bandwidth matrix is not diagonal before the second modulator due to the presence of the first chicane. However, in the typical regime of a small laser bandwidth, $\overline{\delta k^2}_{laser}/\bar{k}^2_{laser} \to 0$, the bandwidth matrix remains mostly diagonal throughout the beamline and one can estimate the bunching bandwidth generated in the EEHG scheme as

$$\left(\frac{\overline{\delta k^2}}{\bar{k}^2}\right)^{(n)}_{\text{EEHG}} \approx \frac{n+2}{n^2}\frac{\overline{\delta k^2_\varphi}}{\bar{k}^2_\varphi}, \quad n\left(\frac{\delta E_1}{\delta E_2}\right)^2\frac{\overline{\delta k^2_\varphi}}{\bar{k}^2_\varphi} \ll 1. \quad (46)$$

This scaling indicates that the relative bunching bandwidth reduces as $1/\sqrt{n}$ at large harmonic numbers, same as for the HGHG scheme.

4.3. Triple modulator–chicane (TMC)

The straightforward generalization of the EEHG scheme can be done by introducing additional stages, each consisting of a modulator and a chicane. The scheme consisting of three such stages and called "triple modulator–chicane" (TMC) was proposed in Ref. [22] and studied in more details in Ref. [23]. Each stage is designed to produce significant modulation at higher harmonic number. The schematics of the TMC scheme is presented in Fig. 5.

The energy modulation at each stage is equal to $\delta E_{1,2,3}$ and the chicanes' strengths are $\xi_{1,2,3}$. The scheme described in Ref. [22] assumed the second chicane to have negative strength $\xi_2 = -\xi_1$. However, it is not required for the performance of the scheme and all the chicanes can be positive. Choosing negative or positive values of the chicane strength defines whether one should track harmonics with either positive or negative wavenumbers so that the energy modulation wavevector is upshifted by each chicane. The schematics of the modulation transform in the TMC scheme with positive chicanes only is shown in Fig. 5.

We design the TMC scheme assuming that undulators introduce modulation at the $n_{1,2,3}$th laser harmonic number. These integer numbers can be either positive or negative. The purpose of the first and the second chicane is to increase k_E of the existing modulation to the value of anticipated modulation in the following undulator. The last chicane recovers imposed modulation as the longitudinal bunching same as in the HGHG and the EEHG schemes. This description allows one to find optimal conditions for the chicane strengths

$$\frac{\partial}{\partial_{k_E}}\left(J_{n_1}(|k_E\delta E_1|)f^0_{\mathbf{k}}(k_z, k_E)\right)\Big|_{(k_E^{(n_1)})_{\max}} = 0, \quad (47)$$

$$(k_E^{(n_1)})_{\max} - \xi_1 n_1 k_z^0 = \frac{\mu_{n_1+n_2,1}}{\delta E_2}, \quad (48)$$

$$\frac{\mu_{n_1+n_2,1}}{\delta E_2} - \xi_2(n_1+n_2)k_z^0 = \frac{\mu_{n_1+n_2+n_3,1}}{\delta E_3}, \quad (49)$$

$$\frac{\mu_{n_1+n_2+n_3,1}}{\delta E_3} - \xi_3(n_1+n_2+n_3)k_z^0 = 0. \quad (50)$$

These expressions are similar to the ones presented in Ref. [23] except for the order of the Bessel function maxima. However, the results agree in the limit $|n_1| \ll |n_2| \ll |n_3|$.

Please cite this article in press as: N.A. Yampolsky, Dynamics of modulated beams in spectral domain, Nuclear Inst. and Methods in Physics Research, A (2017), http://dx.doi.org/10.1016/j.nima.2017.07.008.

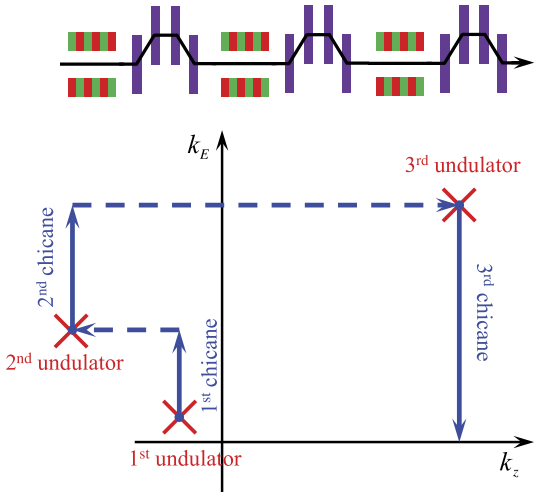

Fig. 5. (Color online) Schematics for the modulation transform in the TMC scheme.

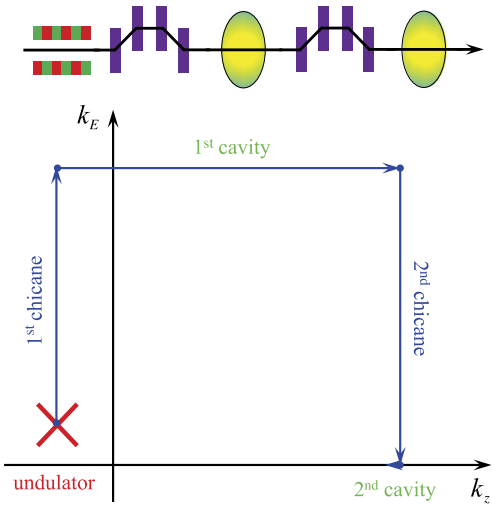

Fig. 6. (Color online) Schematics for the modulation transform in the CHG scheme.

It is reasonable to assume the energy modulation amplitudes to be the same at each stage. Then according to Eq. (49) the sign of the second chicane depends only on the choice of harmonics at each stage of the TMC scheme, $\mathrm{sign}(\xi_2) = -\mathrm{sign}(n_1+n_2)$ which supports the diagram shown in Fig. 5.

The parameters of the TMC scheme can be optimized to result in the most efficient harmonic generation in the second and the third undulator. At the same time, the harmonic generation efficiency in the first undulator depends only on the modulation amplitude and it is the largest for low harmonics. Therefore, we assume $n_1 = -1$ to achieve high performance with the smallest rms energy growth. Then the bunching factor at $-1+n_2+n_3$ harmonic for the optimized scheme is equal to

$$|f_{\mathbf{k}}((-1+n_2+n_3)k_z^0,0)| = J_1(\mu_{1,1})J_{n_2-1}(\mu_{n_2-1,1})J_{n_2+n_3-1}(\mu_{n_2+n_3-1,1}) \approx \approx \frac{0.26}{|(n_2-1)(n_2+n_3-1)|^{1/3}}. \quad (51)$$

The advantage of the TMC scheme is in reduction of the chicane strength compared to the EEHG. That allows to reduce nonlinear effects, coherent synchrotron radiation (CSR) fields, and debunching due to ISR-induced energy spread inside the bends [21].

4.4. Compressed harmonic generation (CHG)

The compressed harmonic generation (CHG) scheme was proposed to generate short wavelength bunching through the longitudinal bunch compression [11]. This effect can be understood by considering the invariant (23). If the beamline is designed to compress the bunch, the bunching wavelength decreases to keep the number of modulation periods within the bunch fixed. Such a scenario can be realized by passing the beam through the RF cavity which introduces the energy chirp and the following bunch compression in the chicane. As it was noticed in Ref. [20], such a design requires strong RF cavities to introduce significant compression without smearing out the resulting bunching factor. Alternatively, the resulting bunching smearing can be avoided at small amplitudes of the energy modulation. However, the amplitude of the imposed modulation is small in this case, similar to the HGHG scheme.

The dynamics of the modulation in the CHG scheme can be tracked in the spectral domain similar to other seeding schemes. RF cavity changes the longitudinal component of the beam modulation wavevector $k_z = k_z^0 - \alpha k_E^0$ according to Eq. (42). The change of the longitudinal wavenumber is proportional to k_E component of the modulation. That implies that the largest change of the modulation longitudinal wavenumber can be reached at small laser-induced energy modulations since $k_E \propto 1/\delta E$. At the same time, the amplitude of the laser-induced energy modulation cannot be much smaller than the rms beam energy spread to provide a large amplitude of the modulation as follows from Eq. (34). Therefore, the largest change in the longitudinal wavenumber of strong enough modulation is limited to $\Delta k_z \sim \alpha/\sigma_E$, which requires strong RF cavities for significant compression of the modulation (increasing the longitudinal wavenumber by an order of magnitude).

To overcome this limit of the CHG scheme, the second chicane was introduced in the beamline [11]. The first chicane increases k_E component of the modulation so that the following cavity would result in a larger shift of the longitudinal wavenumber k_z as follows from Eq. (42). Once the longitudinal wavenumber of the modulation is increased, the second chicane is used to the recover modulation as purely longitudinal bunching. The second RF cavity can be optionally added to the beamline to eliminate the energy chirp from the beam. This cavity does not change the longitudinal wavenumber of modulation ($k_E = 0$ for longitudinal bunching) and therefore, does not affect the beam bunching once it has been created. The schematics of the described scheme is presented in Fig. 6. The sequence of the RF cavities and chicanes duplicates the design described in Ref. [11]. The final bunching is recovered from the $n = -1$ harmonic of the laser modulation in order to utilize chicanes with positive energy dispersion.

The scheme showed in Fig. 6 is designed to transform the initial modulation having a given wavenumber $\mathbf{k}^0 = (-\bar{k}_{laser}, (k_E^{(n)})_{\max})^T$ into the longitudinal bunching having the wavevector $\mathbf{k} = (M\bar{k}_{laser}, 0)^T$, where M is the modulation compression factor. Such a transform can be accomplished with a linear beamline consisting of two chicanes and the RF cavity accelerating the beam at zero crossing

$$\mathbf{k} = \left(R_{\mathrm{chicane2}} R_{\mathrm{cavity1}} R_{\mathrm{chicane1}}\right)^{-T} \mathbf{k}^0. \quad (52)$$

Two equations relating components of the modulation wavevector provide relationships between three parameters of the beamline (dispersions of two chicanes and the RF cavity strength). Assuming that the amplitude of the energy modulation significantly exceeds the rms beam energy, *i.e.* $(k_E^{(n)})_{\max} = \mu_{11}/\delta E$, one finds

$$\xi_1 = \frac{M+1}{-\alpha_1} - \frac{\mu_{11}}{\delta E}, \quad (53)$$

$$\xi_2 = \frac{M+1}{M}\frac{1}{-\alpha_1}. \quad (54)$$

Note that the required cavity strength is negative to ensure positive chicane dispersion. Also note that the strengths of both chicanes are inversely proportional to the amplitude of the RF field. Therefore, this

Please cite this article in press as: N.A. Yampolsky, Dynamics of modulated beams in spectral domain, Nuclear Inst. and Methods in Physics Research, A (2017), http://dx.doi.org/10.1016/j.nima.2017.07.008.

scheme is a subject for parameters study to ensure that all the elements can be made linear enough.

The bunching bandwidth can be estimated using invariant (25). The imposed modulation is mostly longitudinal, $\bar{k}^2_{laser}\sigma_z^2 \gg \mu_{11}^2\sigma_E^2/(\delta E)^2$, so the compression can also be considered as mostly longitudinal. Then the relative bandwidth of the modulation is preserved along the linear beamline and one can estimate CHG bandwidth as

$$\left(\frac{\overline{\delta k^2}}{\bar{k}^2}\right)^{(M)}_{\mathrm{CHG}} \approx \frac{\overline{\delta k^2}_{laser}}{\bar{k}^2_{laser}}. \tag{55}$$

The relative bunching bandwidth mirrors the relative bandwidth of the laser pulse and it does not depend on the beam compression factor M. Note that this scheme requires smaller laser bandwidth compared to HGHG and EEHG schemes in order to achieve the same bandwidth of the resulting bunching.

5. Conclusions

In this paper we have developed the formalism which quantitatively describes dynamics of modulated beams. This formalism is based on the spectral distribution function which is equal to the Fourier transform of the beam distribution function in the 6D phase space. The introduced spectral distribution is localized in some region of the spectral domain which makes possible to characterize it with a limited number of parameters such as the average wavevector of the modulation and the bandwidth matrix. The key advantage of the proposed formalism is based on the observation that any given spectral component of the distribution remains as a single component under linear transforms indicating that the topology of the spectral distribution remains the same along any linear beamline. As a result, the characteristic parameters of the spectral distribution transform linearly.

The developed formalism has two main advantages compared to alternative approaches based on trailing coordinates of each individual electron in the phase space. First, the formalism quantifies the main parameters of the modulated beams which introduces suitable metrics characterizing modulated beams. Different competing schemes can be easily compared to each other using this metrics. Second, the developed formalism describes the change of the spectral parameters along arbitrary linear beamline. The spectral parameters transform linearly and their change is solely described with the conventional beam transform matrix. As a result, the developed description of the modulated beams dynamics is full and self-consistent.

This description estimates the bandwidth of the resulting modulation which allows to determine whether some proposed scheme satisfies requirements for a given application. As an example, we have considered several laser based schemes proposed for the XFEL seeding and found the output bunching bandwidth for a laser with random phase noise.

Note that the description of the beam in the spectral domain is a useful concept for a wide class of problems in Beam Physics. It can be applied for solving homogeneous linear problems [21] or analyzing linear instabilities.

Acknowledgments

Author is thankful to B. E. Carlsten for useful discussions and suggestions. This work is supported by the US Department of Energy through the LANL/LDRD program.

Appendix. Interpretation of modulation invariants

Invariants (24) of the modulated beam dynamics can be interpreted using the eigen-emittance concept [18]. According to Williamson's theorem [24], any real symmetric positively defined matrix Σ can be diagonalized with a symplectic matrix A, *i.e.* $A^T J A = J$, through the transform

$$A(s)\Sigma(s)A^T(s) = \Lambda, \qquad \Lambda_{ij} = 0 \ \text{ for } i \neq j, \tag{A.1}$$

$$\Lambda_{2n-1,2n-1}\cdot\Lambda_{2n,2n} = \epsilon^{(n)}_{\mathrm{eig}}. \tag{A.2}$$

In case of the rms beam matrix $\Sigma = \langle\zeta\zeta^T\rangle$, $\epsilon^{(n)}_{\mathrm{eig}}$ are called the "eigen-emittances" and they remain constant along the linear beamline. Williamson's theorem can be interpreted in two ways. The first interpretation states that any arbitrary beam matrix can be diagonalized throughout appropriate beam optics which transform matrix is equal to $R = A$. Alternatively, matrix A can be considered as a canonical transformation of the canonical variables $\zeta_{\mathrm{eig}} = A\zeta$ in which the beam matrix becomes diagonal. Williamson's Theorem states that the transform matrix A can be chosen in such a way that the diagonal terms come in pairs, *i.e.* $\Lambda_{2n-1,2n-1} = \Lambda_{2n,2n}$. However, that requires renormalization of the canonical variables so that they have equal dimensions. As a result, the elements of the beam matrix are lacking clear physical interpretation such as rms bunch size or angular spread. Alternatively, we chose transform matrix A which only decouples the eigen-phase planes but does not necessarily diagonalize the beam matrix associated with these planes

$$A(s)\Sigma(s)A^T(s) = diag\left(\Sigma^{(n)}(s)\right), \tag{A.3}$$

$$\det\left(\Sigma^{(n)}(s)\right) = \epsilon^{(n)}_{\mathrm{eig}} = inv, \tag{A.4}$$

where $\Sigma^{(n)}(s)$ is 2×2 beam matrices corresponding to nth eigen-phase plane.

The concept of the eigen-phase planes provides simple picture for bunch dynamics since particle motion in different eigen-phase planes is decoupled from each other. Note that the decomposition into the eigen-phase space coordinates is not unique and so the beam dynamics within a given eigen-phase plane depends on the choice the of the eigen-coordinates. For example, if one chooses the eigen-coordinates $\zeta_{\mathrm{eig}} = A(s)\zeta$ so that $A(s) = A(s_0)R(s,s_0)^{-1}$ then the beam is stationary in this rotating frame, *i.e.* $\partial_s\Sigma^{(n)}(s) = 0$. This choice of rotating phase space may be not the simplest description. For example, quad focusing and beam divergence are easier to describe in a stationary frame.

The eigen-phase plane concept also simplifies description of the modulated beams. The change of the phase space coordinates to the eigen-coordinates $\zeta_{\mathrm{eig}} = A(s)\zeta$ defines the wavevector of the modulation in this frame $\mathbf{k}_{\mathrm{eig}}(s) = A^{-T}(s)\mathbf{k}(s)$. One can naturally define the projections of the wavevector onto the eigen-phase planes as $\mathbf{k}^{(n)}_{\mathrm{eig}} = ((k_{\mathrm{eig}})_{2n-1},(k_{\mathrm{eig}})_{2n})^T$. These projections of the wavevector evolve independently from each other since particle dynamics within different eigen-phase planes is not coupled. Moreover, if one chooses rotating frame such as $A(s) = A(s_0)R(s,s_0)^{-1}$ then the wavevector of the modulation in this frame does not change along the beamline. As a result, the entire distribution function remains constant in this frame since each individual Fourier harmonic does not change. The choice of the rotating frame which does not eliminate particle dynamics within each eigen-phase plane, $\partial_s\Sigma^{(n)}(s) \neq 0$, also implies evolution of the eigen-wavevector, $\partial_s\mathbf{k}^{(n)}(s) \neq 0$. However, in this case one can find the invariants

$$\left(\mathbf{k}^{(n)}(s)\right)^T\Sigma^{(n)}(s)\mathbf{k}^{(n)}(s) = inv. \tag{A.5}$$

These invariants can be interpreted as the rms phase of the modulation across each eigen-phase plane area.

The same invariants can be formulated in the lab frame without introduction of the eigen-coordinates. In this case the invariants read as

$$\mathbf{k}^T(s)J\left(\Sigma^{-1}(s)J\right)^{2n+1}\mathbf{k}(s) = inv, \quad n = 1,2,\ \ldots\ dim(\Sigma)/2. \tag{A.6}$$

There is an infinite number of invariants but the number of the functionally independent ones is equal to the dimension of the space describing

Please cite this article in press as: N.A. Yampolsky, Dynamics of modulated beams in spectral domain, Nuclear Inst. and Methods in Physics Research, A (2017), http://dx.doi.org/10.1016/j.nima.2017.07.008.

the beam dynamics, *i.e.* is equal to 3 in general case. Moreover, the preservation of the rms modulation phase across each eigen-phase plane leads to the preservation of the rms modulation phase across the entire phase space volume

$$\sum_{n=1}^{dim(\Sigma)/2} \left(\mathbf{k}^{(n)}\right)^T \Sigma^{(n)} \mathbf{k}^{(n)} = \mathbf{k}^T \Sigma \mathbf{k} = inv. \tag{A.7}$$

References

[1] W. Ackermann, et al., Operation of a free-electron laser from the extreme ultraviolet to the water window, Nat. Photonics 1 (2007) 336.
[2] P. Emma, et al., First lasing and operation of an angstrom-wavelength free-electron laser, Nat. Photonics 4 (2010) 641.
[3] T. Shintake, et al., A Compact free-electron laser for generating coherent radiation in the extreme ultraviolet region, Nat. Photonics 2 (2008) 555.
[4] M. Altarelli, et al., XFEL: The European X-ray Free-Electron Laser Technical Design Report. Preprint DESY 2006-097 (DESY, 2006).
[5] E. Allaria, et al., Two-stage seeded soft-X-ray free-electron laser, Nature Photon. 7 (2013) 913.
[6] A.M. Kondratenko, E.L. Saldin, Generation of coherent radiation by a relativistic electron beam in an ondulator, Part. Accel. 10 (1980) 207.
[7] J. Feldhaus, E.L. Saldin, J.R. Schneider, E.A. Schneidmiller, M.V. Yurkov, Possible application of X-ray optical elements for reducing the spectral bandwidth of an X-ray SASE FEL, Opt. Commun. 140 (1997) 341.
[8] G. Geloni, V. Kocharyan, E. Saldin, A novel self-seeding scheme for hard X-ray FELs, J. Modern Opt. 58 (2011) 1391.
[9] L.H. Yu, Generation of intense uv radiation by subharmonically seeded single-pass free-electron lasers, Phys. Rev. A 44 (1991) 5178.
[10] G. Stupakov, Using the beam-echo effect for generation of short-wavelength radiation, Phys. Rev. Lett. 102 (2009) 074801.
D. Xiang, G. Stupakov, Echo-enabled harmonic generation free electron laser, Phys. Rev. ST Accel. Beams 12 (2009) 030702.
[11] S.G. Biedrona, S.V. Miltona, H.P. Freund, Modular approach to achieving the next-generation X-ray light source, Nucl. Instrum. Methods A 475 (2001) 401.
[12] B. Jiang, J.G. Power, R. Lindberg, W. Liu, W. Gai, Emittance-exchange-based high harmonic generation scheme for a short-wavelength free electron laser, Phys. Rev. Lett. 106 (2011) 114801.
[13] B.E. Carlsten, et al., New X-ray free-electron laser architecture for generating high fluxes of longitudinally coherent 50 keV photons, J. Modern Opt. 58 (2011) 1374.
[14] L.-H. Yu, et al., High-gain harmonic-generation free-electron laser, Science 289 (2000) 932.
[15] Y.-E. Sun, P. Piot, A. Johnson, A.H. Lumpkin, T.J. Maxwell, J. Ruan, R. Thurman-Keup, Tunable subpicosecond electron-bunch-train generation using a transverse-to-longitudinal phase-space exchange technique, Phys. Rev. Lett. 105 (2010) 234801.
[16] D. Xiang, et al., Demonstration of the echo-enabled harmonic generation technique for short-wavelength seeded free electron lasers, Phys. Rev. Lett. 105 (2010) 114801.
[17] P. Muggli, V. Yakimenko, M. Babzien, E. Kallos, K.P. Kusche, Generation of trains of electron microbunches with adjustable subpicosecond spacing, Phys. Rev. Lett. 101 (2008) 054801.
[18] A.J. Dragt, F. Neri, G. Rangarajan, General moment invariants for linear Hamiltonian systems, Phys. Rev. A 45 (1992) 2572.
[19] M. Cornacchia, P. Emma, Transverse to longitudinal emittance exchange, Phys. Rev. ST Accel. Beams 5 (2002) 084001.
[20] D. Ratner, A. Chao, Z. Huang, Two-chicane compressed harmonic generation of soft x rays, Phys. Rev. ST Accel. Beams 14 (2011) 020701.
[21] N.A. Yampolsky, B.E. Carlsten, Beam debunching due to ISR-induced energy diffusion, Nuclear Inst. Methods Phys. Res. (2017). http://dx.doi.org/10.1016/j.nima.2017.06.023. in press.
[22] D. Xiang, G. Stupakov, Triple modulator-chicane scheme for seeding sub-nanometer x-ray free-electron lasers, New J. Phys. 13 (2011) 093028.
[23] E. Hemsing, D. Xiang, Cascaded modulator-chicane modules for optical manipulation of relativistic electron beams, Phys. Rev. ST-AB 16 (2013) 010706.
[24] J. Williamson, On the algebraic problem concerning the normal forms of linear dynamical systems, Amer. J. Math. 58 (1936) 141.

Please cite this article in press as: N.A. Yampolsky, Dynamics of modulated beams in spectral domain, Nuclear Inst. and Methods in Physics Research, A (2017), http://dx.doi.org/10.1016/j.nima.2017.07.008.